Correspondence to:
Q. Zhang and W. Li,
qzhang@pku.edu.cn;
wenhong.li@duke.edu

Changes in Hourly Extreme Precipitation Over Eastern China From 1970 to 2019 Dominated by Synoptic-Scale Precipitation

Chan-Pang Ng[1] [ORCID], **Qinghong Zhang[1]** [ORCID], **and Wenhong Li[2]** [ORCID]

[1]Department of Atmospheric and Oceanic Sciences, School of Physics, Peking University, Beijing, China, [2]Earth and Ocean Sciences, Nicholas School of the Environment, Duke University, Durham, NC, USA

Abstract Because of its dense population, extreme precipitation, in particular hourly extreme precipitation (HEP), is receiving increasing attention from both academic and public bodies in eastern China. Based on a continuous 50-year record of hourly precipitation and reanalysis data, we show here for the first time that changes in the HEP occurrence are dominated by changes in the duration of the Meiyu front system. Further analyses reveal that greater occurrence of HEP in northeastern China, the lower reach of Yangtze River, and southern China during the warm season is largely due to a longer duration of the post-Meiyu I stage when Meiyu front stays in northern China and meridional circulation dominates the eastern coastal area of China. These results improve our understanding of the changing behavior of extreme rainfall in China and shed light on the prevention of flash floods.

Plain Language Summary Hourly extreme precipitation (HEP) events can lead to instant disasters, such as flash floods or waterlogging, resulting in huge losses of human life and property in a short period. Most previous studies have focused on daily extreme precipitation in China. Our study examined how and why HEP has changed in the past half-century. We show that changes in the number of HEP events are mainly contributed by synoptic-scale extreme precipitation in the warm season over eastern China. Furthermore, as the Meiyu front stays longer over northern China in recent years, the number of HEP events have increased in July and August in the lower reach of Yangtze River, northeastern and southern China. These results improve understanding of the response of HEP to climate change and imply that synoptic weather systems might be more important for changes in the occurrence of HEP than local-scale weather systems.

1. Introduction

How extreme precipitation events respond to climate change (Miao et al., 2016) is a hot but complicated issue in the field of atmospheric science (Hansen et al., 2010; Jones et al., 2012; Lawrimore et al., 2011; Rohde et al., 2013). Hourly extreme precipitation (HEP) can lead to instant disasters such as a flash flood that results in a huge loss of human life and property in a short period (Brooks & Stensrud, 2000; Parry et al., 2007). As the economy has developed, an increasing number of people migrated to eastern China, in particular along with the coastal areas, there is an urgent need to understand how and why HEP has changed in eastern China to provide a theoretical basis for improving extreme rainfall prediction and decision-making capabilities.

In a warmer climate, the thermodynamic effect plays a major role in determining the annual mean extreme precipitation on a global level (Emori & Brown, 2005), while changes in atmospheric circulation, are thought to be important on local and regional scales; but detailed dynamic mechanisms are not well understood in many regions (Vallis et al., 2015). Warming not only affects radiative properties and the amount of atmospheric water vapor, but also changes atmospheric dynamics (Chou & Chen, 2010; Gao et al., 2016; Vallis et al., 2015; You et al., 2019). These factors usually interwind to affect extreme precipitation in China, it is therefore difficult to quantitatively determine the physical mechanisms' key to the changes in extreme precipitation. Previous analysis found that changes in the HEP intensity were largely related to surface air temperature in the southeastern coastal area of China, but not in northern China (Yu & Li, 2012). Moreover, the weakening of the summer monsoons was thought to contribute to the decreased number of daily extreme precipitation over central-eastern China and increased in the Yangtze River basin (Y. Wang &

Zhou, 2005); however, the increased number of extreme precipitation in other areas of eastern China could not be explained by dynamically driven alone.

Synoptic-scale precipitation is generally associated with large-scale weather systems dominated by dynamic processes, while local precipitation is often caused by local-scale weather systems primarily controlled by thermal effects (Guo et al., 2017; Houze Jr, 2014). Given the complexity of physical mechanisms on precipitation, it is useful to simplify the question by dividing precipitation into different types. Guo et al. (2017) suggested that dividing hourly precipitation into synoptic and local scales is a simple but effective way to better understand the causes of changes in precipitation.

Although previous studies have discussed climatology and long-term trend of HEP (Luo et al., 2016; Yu & Li, 2012; H. Zhang & Zhai, 2011), none of them investigate detailed mechanisms behind the changes of HEP in China using up-to-date gauge data. Our study examines the characteristics of HEP and its changes and analyzes what causes such changes in view of synoptic- and local-scale precipitation.

2. Data and Method

An hourly rainfall data set was obtained from the National Meteorological Information Center, China Meteorological Administration, which maintained rain-gauge records at 2,435 stations in mainland China from 1951 to 2019. We adopted the criteria of the relocation problem and the continuous valid record after Zhai et al. (2005) and H. Zhang and Zhai (2011). Observational data were not included if a station was moved more than 20 horizontal kilometers from the original location or reinstalled in elevation 50 m or more during the study period, or the availability rate, defined as the rate of correct and valid records out of the entire records in the warm season (May–September) in any year, was less than 80%. Since the availability rate of data is greater than 97.5% and more stable after 1970, the analyses were restricted to the period 1970–2019 to ensure that the records were reliable and covered sufficient observatories in eastern China from 1970 to 2019. A total of 741 stations passed quality control (Figure 1a).

As the primary monsoon system affecting China, East Asian summer monsoon (EASM), a subtropical monsoon in which the low-level winds reverse primarily from northerly in winter to southerly in summer (Ding & Chan, 2005; B. Wang & LinHo, 2002), has different rainfall stages, i.e., spring, pre-Meiyu, Meiyu, mid-summer, and fall (Chiang et al., 2017; Kong et al., 2017). To quantify the synoptic-scale circulation at different monsoon stages, we used reanalysis data from the National Centers for Environmental Prediction/National Center for Atmospheric Research (NCEP/NCAR) (Kalnay et al., 1996). This reanalysis data covered the period from 1948 to the present day, with four values per day and a spatial resolution of 2.5° latitude × 2.5° longitude. The pseudo-equivalent potential temperature (θ_e) (Bolton, 1980) and horizontal winds at 850 hPa were calculated at 6-h basis.

2.1. Definition of HEP

In the study, HEP events were defined at each station as precipitation amounts greater than the 95th percentile of the hourly rainfall (rain rate greater than 0.1 mm h^{-1}) in the warm season (May-September) during 1970–2019 (Figure S1). The overall results will not change much if we choose the 90th percentile as the criteria to define HEP (not shown).

2.2. Determination of Local- and Synoptic-Scale HEP (L-HEP and S-HEP)

We defined L-HEP and S-HEP following Guo et al. (2017) with modifications. An HEP was considered as an L-HEP at a weather station when the HEP met the following two criteria: within a 200 km radius[1] around the station, there had to be more than five stations besides the station itself (criteria 1), and the percentage of stations with rainfall record had to be less than 20% (criteria 2). If an HEP event only satisfied the first

---

[1]To include more stations within the radius for effectively calculating different scales of hourly precipitation, 200-km radius is chosen here instead of 150-km in Guo et al. (2017) although the overall results do not change.
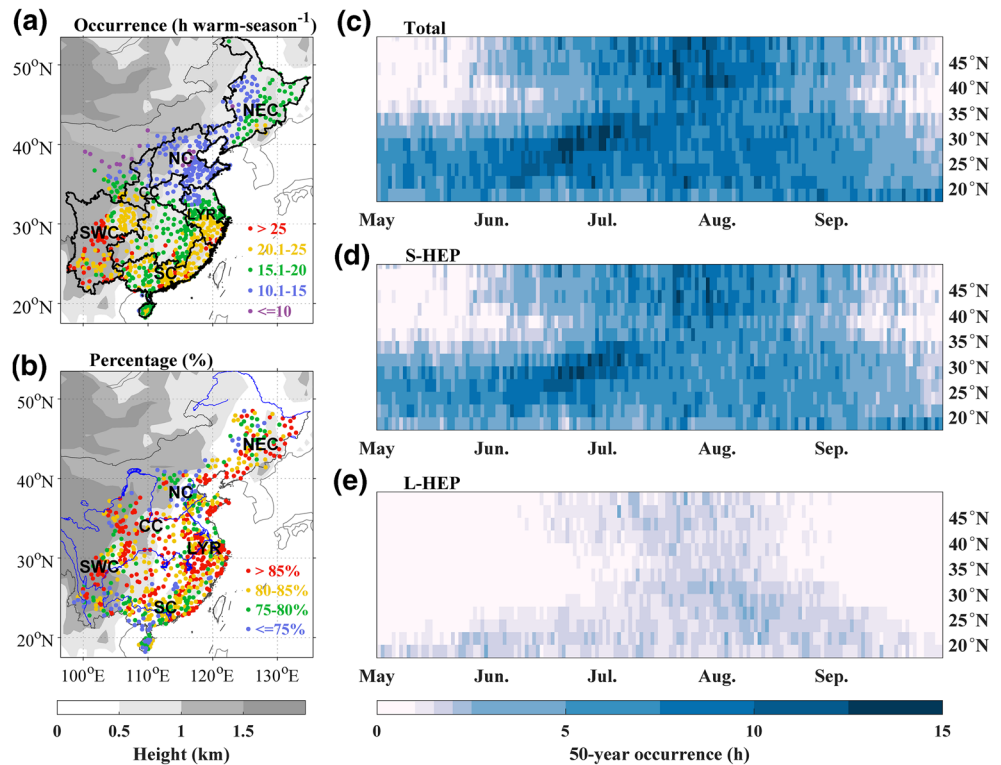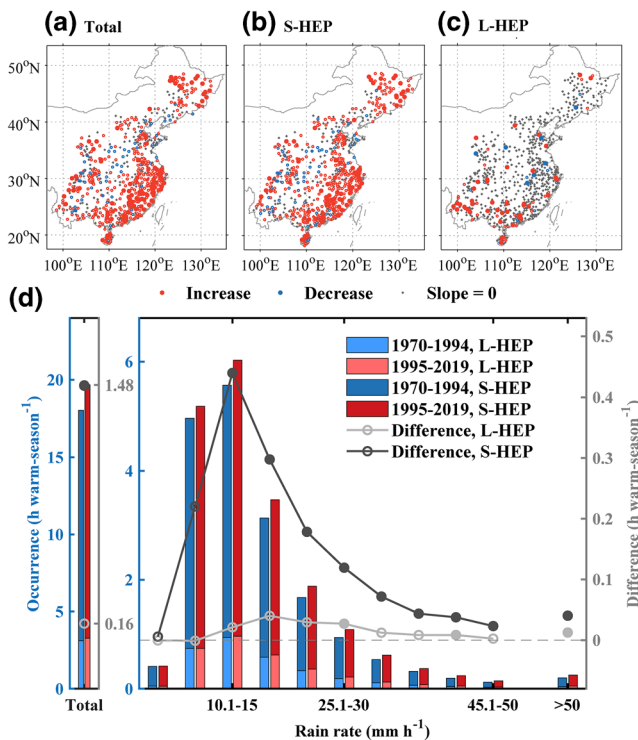
Figure 1. (a) Mean occurrence of hourly extreme precipitation (HEP; unit: h warm-season^{-1}) events at each gauge station in the warm season (May–September) during 1970–2019, and (b) percentage of synoptic-scale HEP (S-HEP) events out of the total HEP events. Latitudinal variation of occurrence of station averaged (unit: h) (c) total HEP, (d) S-HEP, and (e) local-scale HEP (L-HEP) from May–September during the period of 1970–2019. The occurrences of HEP, S-HEP, and L-HEP are plotted onto 2.5° latitude × 1-day grids. In (a)–(b), gray shading indicates the terrain altitude in kilometer. For clarity, northeastern China (NEC), northern China (NC), central China (CC), southwestern China (SWC), the lower reach of Yangtze River (LYR), and southern China (SC) defined by their geographic locations are labeled in black.

criteria but not the second, it was considered as an S-HEP. Note, only stations at which the precipitation records meet the first criteria can be used to distinguish between L-HEP and S-HEP events; as a result, of the 741 stations passing quality control, 716 stations are chosen (Figures 1b–1e, and 2).

2.3. Self-Organizing Maps (SOMs)

To further understand the changing behavior of the duration and averaged daily HEP frequency in the warm season from 1970 to 2019, a clustering method SOM analysis (Johnson, 2013; Kohonen, 2001; Kohonen et al., 1996) was applied to the HEP for all the 741 stations. The occurrence of HEP is first counted in a day, and calculated into a 50-year average or a 25-year average for the 1970–1994 and 1995–2019 period for each day; a 5-day moving average is then conducted before utilizing the SOMs technique to avoid high-frequency noise and better capture the characteristics of HEP patterns at different monsoon stages. The HEP events were classified according to the five monsoon stages in the warm season. The SOM method is a neural network-based cluster analysis that classifies a high-dimensional data set into representative patterns, using a neighborhood function to topologically order the high-dimensional input and group similar clusters together (Kohonen & Somervuo, 1998). Unlike other clustering methods (e.g. k-means [Lin & Chen, 2006] and Ward's methods [Bao & Wallace, 2015; Lin & Chen, 2006]), SOMs could extract more robust and distinctive topology information. This method is ideally suited given the discreteness of intraseasonal stages and abrupt transitions evident in the EASM (Chiang et al., 2017). The SOMs function in the MATLAB 2018b Deep Learning Toolbox (https://www.mathworks.com/help/deeplearning/index.html) was used to cluster the data and reduce their dimensionality.

Figure 2. Trends in occurrence of (a) total hourly extreme precipitation (HEP), (b) synoptic-scale HEP (S-HEP), and (c) local-scale HEP (L-HEP) at each station in the warm season during the period 1970–2019. Black plus signs, red circles, and blue circles represent that slope of 0, an increase, and a decrease, respectively. Stations with significant trends at the 95.0% confidence level have large dots. (d) Comparison of the S-HEP and L-HEP occurrences (unit: h warm-season^{-1}) at 11 rainfall intensities and total rainfall amount in the first (1970–1994) and second (1995–2019) 25-year periods. The left of the *Y*-axis (blue) indicates the occurrence and the right of the *Y*-axis (gray) indicates the difference between the first and second periods. The difference with statistical significance at the 95.0% confidence level are represented by solid dots. The *X*-axis shows the total amount of rainfall for an hour, rainfall intensity in 0.1–5, 5.1–10, 10.1–15 mm/h, ..., 45.1–50 mm/h, and >50 mm/h, respectively.

3. Results
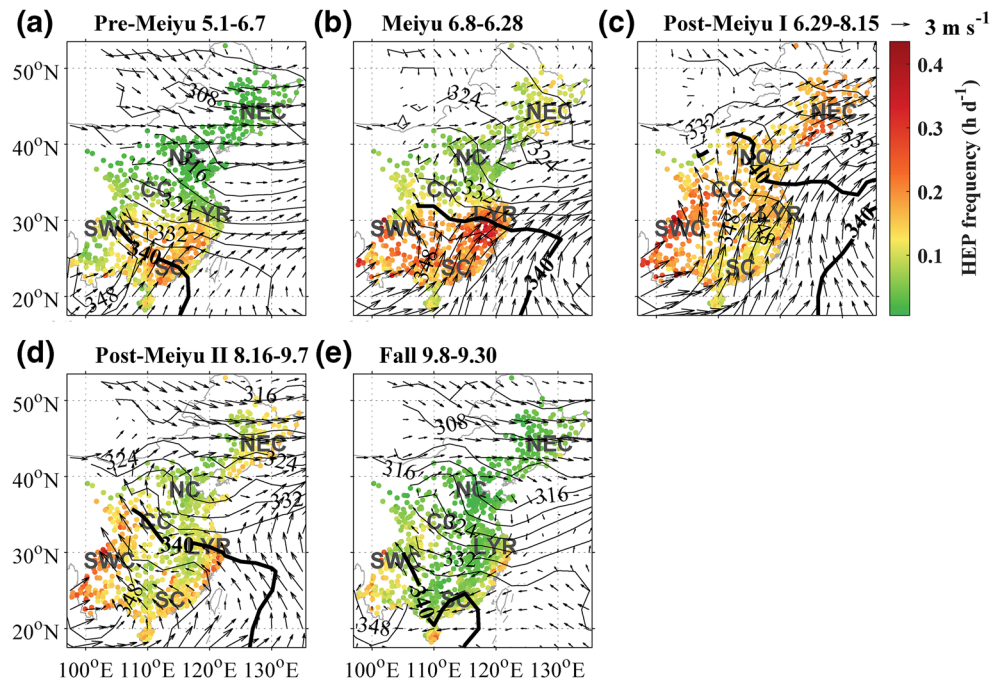
3.1. Characteristics of HEP

Figure 1a shows the mean occurrence of HEP in the warm season for the 741 stations over eastern China during 1970–2019. The HEP occurrence decreases from south to north of eastern China and varies between 7.20 and 41.18 h across the region. S-HEP events account for more than 85.0% of total HEP in most areas, in particular over the lower reach of the Yangtze River (LYR) (Figure 1b). The minimum percentage of S-HEP over total HEP is about 61.7%, in northern China (NC).

In eastern China, the main precipitation system in the warm season is usually associated with the shift of the Meiyu front and occasionally tropical cyclones (TCs), we thus analyze the latitude variation of the occurrence of HEP, S-HEP, and L-HEP, respectively, from May to September during 1970–2019 (Figures 1c–1e). Along with the monsoon onset, HEP starts in May at the low latitude region (south of 30°N). During June and July, the high-occurrence of HEP (i.e., HEP is greater than 10-h) moves from southern to northern China and retreats southward quickly in late August. During the warm season, HEP events appear more frequently in the low latitude region (south of 30°N) compared to the middle (30°N–38°N) and high latitude (north of 38°N) regions. The latitude variation of S-HEP (Figure 1d) is similar to that of HEP (Figure 1c) from May to September, indicating that changes in synoptic-scale HEP dominate changes in total HEP.

3.2. Changes in the Occurrence of HEP

Figures 2a–2c show the trends of occurrence of HEP, S-HEP, and L-HEP in the warm season at each station during 1970–2019, respectively. The Mann-Kendall test with Sen's slope was used here (Kendall, 1975; Mann, 1945; Sen, 1968). Positive trends of total HEP are observed in the SC, LYR, and northeastern China (NEC) regions, generally in consistent with the results of H. Zhang and Zhai (2011) who analyzed fewer gauge data ending at 2000, but more stations are showing an upward trend in our study. Specifically, HEP increases with time in 489 stations, the trends are significant at a 5.0% level for 101 stations in the SC, LYR, and NEC regions. Downward trends are found at 66 stations, but none of them is significant. Of the 741 stations, 161 stations show that the slope is 0 (Figure 2a). Comparing Figures 2a, 2b, and 2c, we find that the positive trend of HEP is mainly due to the increase in S-HEP (Figure 2b). The correlation between the trend in HEP and S-HEP is 0.82, which is much higher than that between the HEP and L-HEP, with a value of 0.17 (Figures 2b–2c).

We further analyze the occurrence changes of HEP, S-HEP, and L-HEP in different rainfall intensity categories and the total amount of rainfall from the first (1970–1994) to the second (1995–2019) 25-year periods (Figure 2d). Among the 11 different rainfall intensities, the highest HEP occurrence occurs when precipitation intensity is within 10.10–15.00 mm h^{-1} in both periods.

Compared with the first 25-year period, the occurrence of total HEP grows by about 9.1% in the second period (left-most bars Figure 2d), and the growth in HEP number is mainly due to the increase in S-HEP. The increasing features in S-HEP and L-HEP are observed in nine rainfall intensity bins, except for the intensity bins in 0.10–5.00 and 5.10–10.00 mm h^{-1} where L-HEP is decreasing. Figure 2d also shows that the occurrence of S-HEP increases the most within the 10.10–15.00 mm h^{-1} rainfall intensity bin, same as total HEP. In summary, the changed occurrence of S-HEP dominates the number of growths in total HEP during the second 25-year period.

Figure 3. Spatial patterns in self-organizing maps analysis of the averaged daily frequency of HEP (unit: h d^{-1}) during the period of 1970–2019. Pattern 1 denotes the "pre-Meiyu" (May 1–June 7). Pattern 2 denotes the "Meiyu" (June 8–June 28). Pattern 3 denotes the "post-Meiyu I" (June 29–August 15). Pattern 4 denotes the "post-Meiyu II" (August 16–September 7). Pattern 5 denotes the "fall" (September 8–September 30). Arrows represent the horizontal wind and black lines represent the pseudo-equivalent potential temperature (unit: K) at 850 hPa, and each line interval is 4 K. The bold line indicates the southern boundary of the Meiyu front.

3.3. What Lead to Changes in HEP?

It has been long known that rainfall in eastern China is closely related to monsoons in the warm season (Ding & Chan, 2005; Tao, 1987). It is necessary to find out if changes in EASM between the first and second 25-year period dominate the changes in the warm-season HEP occurrence over eastern China.

We first show the 50-year climatological pattern of HEP (Figure 3) based on SOMs analyses. The five SOMs HEP nodes reasonably capture the intraseasonal stages of EASM rainfall over eastern China (Chiang et al., 2017; Kong et al., 2017). The rainfall patterns present here are generally in agreement with those in Chiang et al. (2017) and Kong et al. (2017), with slight differences in onset time and duration because we use different precipitation data sets and up-to-date research periods (ending at 2019).

During the pre-Meiyu stage (May 1–June 7), HEP first appears in SC (mainly south of 30°N, Figure 3a). The southerly wind brings moisture from adjacent oceans to SC, favorable to generate HEP events. From June 8 to June 28, the Meiyu front migrates northward to the LYR region at the Meiyu stage (Figure 3b). At the same time, following the monsoon movement, HEP occurs at the east side of the Tibet Plateau, where the Indian summer monsoon (ISM), a tropical monsoon in which the low-level winds reverse from winter easterlies to summer westerlies (Ding & Chan, 2005; B. Wang & LinHo, 2002), joins the EASM to facilitate convection. After the Meiyu stage, the southerly wind continues to strengthen and moves further north. During the post-Meiyu I stage (Figure 3c), the Meiyu front migrates northward to the NC region, leading to the high daily HEP frequency there. Besides, the HEP can be observed in the NEC region, likely due to the mountain topography uplifting airflow (X. Zhang et al., 2012). The SC also has a relatively high averaged daily HEP frequency (around 0.15–0.20 h d^{-1}) in the post-Meiyu I stage, associated with the meridional circulation accompanied by the strong low-level jet that provides moisture and dynamic forcing of convection (Li et al., 2016; Q. Zhang et al., 2017). The averaged daily HEP frequency in SC is not as high as in the pre-Meiyu stage, which is around 0.20–0.25 h d^{-1}. The ISM is strongest in July when the warm and humid
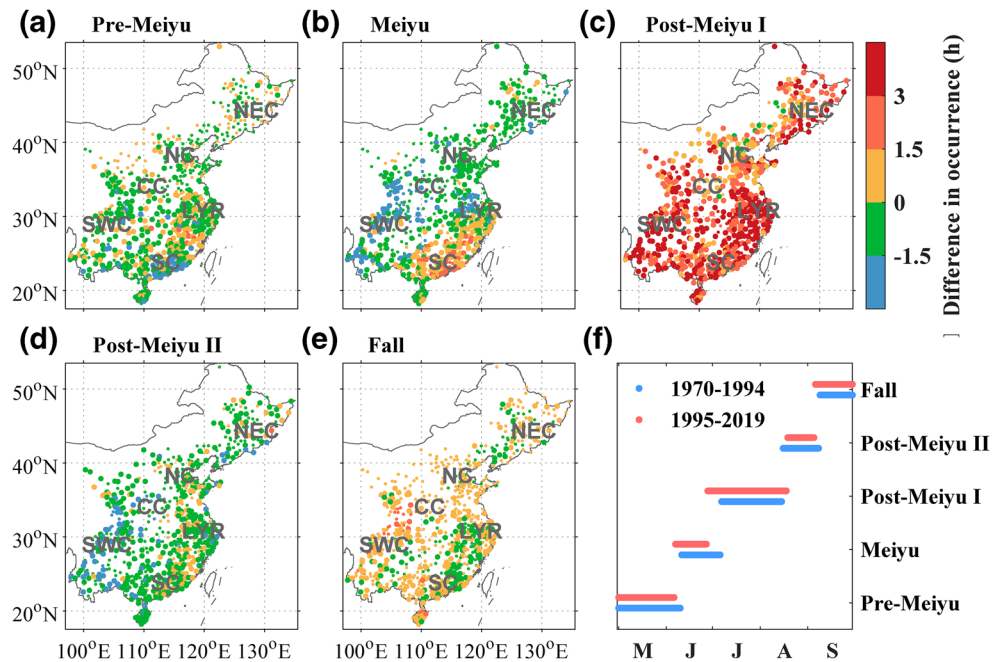
Figure 4. (a)-(e) Differences in occurrence of HEP (unit: h) at each station during the five monsoon intraseasonal stages from 1970–1994 to 1995–2019, and (f) the durations of the five monsoon stages based on self-organizing maps analyses of HEP. In (a)–(e), stations with statistical significance at the 95.0% confidence level are represented by large dots. In (f), red and blue lines represent the periods of pre-Meiyu, Meiyu, post-Meiyu I, post-Meiyu II, and fall stages in 1970–1994 and 1995–2019, respectively.

air mass meets the air mass from the north in southwestern China (SWC) to form the southwest vortex, which may be responsible for the extreme precipitation (Figure 3c) (Chen et al., 2015; X. Wang e al., 2017).

In the post-Meiyu II stage, the 340-K isoline of θ_e, influenced by the weakening of the EASM and the ISM, retreats to LYR, leading to the declines of the averaged daily HEP frequency in both NC and NEC regions (Figure 3d). In the SC region, the dominant winds are southeasterly. The majority of HEP events are observed in the coastal area and SWC. As the monsoons retreat further south in fall (Figure 3e), except for the impact of TCs on the SC and some weak weather systems in individual areas (Luo et al., 2016), HEP events end in most of the areas north of the Yangtze River (Figure 3e). We note that the variation in L-HEP (unit: h d^{-1}) is not obvious (Figure S2), indicating that variation in HEP is mainly due to changes in S-HEP.

However, the onset and duration of HEP in the five stages change from the first (1970–1994) to the second (1995–2019) period. Figure 4 shows the differences in occurrence of HEP in hours (Figures 4a–4e), the beginning/ending dates and duration at each stage (Figure 4f). The pre-Meiyu, Meiyu, and post-Meiyu II stages end early by 4, 9, and 3 days, respectively, whereas the starting dates begin early for the Meiyu, post-Meiyu I, and fall stages in the latter period. Thus, compared to the first 25-year period, the duration of the post-Meiyu I and fall precipitation stages increase by 12 and 3 days, separately, but the pre-Meiyu, Meiyu, and post-Meiyu II stages shorten by 4, 5, and 6 days during 1995–2019. A nonparametric bootstrap method (with a hundred samples) is used for estimating the statistical significance of the difference in each stage's duration (Davison & Hinkley, 1997; Lupu & Maenhaut, 2002; Marchand et al., 2006). Results suggest that the changes in the durations of the five stages from 1970–1994 to 1995–2019 are all significant (Table S1).

Changes in the duration do not necessarily alter the total occurrence of HEP in each monsoon stage, the daily mean of HEP occurrence, that is, the rate of HEP change per day, could also alter; we thus further analyze the relative contributions of the changes in duration and rate of HEP to the total occurrence of HEP from the first to the second 25-year period. Results suggest that from 1970–1994 to 1995–2019, about 97.6% and 70.9% stations show increase in the total occurrence of HEP during the post-Meiyu I and fall stages, separately (Figures 4c and 4e), and 89.2% and 30.7% stations passed significance test. These are largely due to the longer durations in the second 25-year period (Figure 4f); HEP daily frequencies also increase during

the post-Meiyu I and fall stages (Figures S3c and S3e), which contribute to the changes in HEP. Compared to the duration changes, HEP daily frequencies (i.e., the rate of change per unit time) increase at fewer stations, 5.5% and 7.8% stations passing the significance test at the post-Meiyu I and fall stages, respectively.

The patterns of differences in the total occurrence of HEP between 1970–1994 and 1995–2019 are dissimilar among the five stages. Increased HEP occurrence is observed across eastern China in the post-Meiyu I (Figure 4c), and over much of eastern China during the fall stage (Figure 4e), respectively. During post-Meiyu I and fall stages, S-HEP increases by 48.4% and 27.2%, separately (Figures S4–S5). On the contrary, during the other three stages, i.e., the pre-Meiyu (Figure 4a), Meiyu (Figure 4b), and post-Meiyu II (Figure 4d) stages, HEP occurrence either slightly increases or decreases over eastern China from the first to the second 25-year period. HEP events occur more along coastal SC during the Meiyu stage. These phenomena demonstrate that change in the occurrence of HEP in the warm season from 1970–1994 to 1995–2019 is largely due to the changes in HEP occurrence during the post-Meiyu I and fall stages, especially in the post-Meiyu I stage (the national mean contribution is 66.7% in total HEP difference in the warm season), when partly associated with increased TC-induced precipitation (Figure S6).

4. Conclusions

Using long-term measurements of hourly rainfall of 741 stations during 1970–2019 in eastern China and NCEP/NCAR reanalysis data, we examined how and why HEP has changed during the warm season in the past half-century. Our analysis found that climatologically, HEP occurrence varies between 7.20 h and 41.18 h across eastern China in the warm season. During the past 50 years, the occurrence of HEP has increased over NEC, LYR, and SC; such changes of HEP is largely due to changes in occurrence of S-HEP in the warm season.

We carry out SOMs analysis applied to HEP data to identify the timing, duration, and changes of these intraseasonal stages from 1970–1994 to 1995–2019 in order to reveal the HEP changes. Among the five intraseasonal stages of the EASM, the increase of HEP occurrence (total hours in the second 25-year period) mainly occurs in the post-Meiyu I stage when southerly winds dominate eastern China. Compared to 1970–1994, the duration of the post-Meiyu I stage becomes 12 days longer (1995–2019), leading the Meiyu front to stay in NEC and NC longer and S-HEP increase by 48.4%. SC and LYR are dominated by meridional circulation that brings more moisture and HEP events to the regions. These results suggest the relatively important roles of synoptic weather systems and circulation patterns played in the HEP events in recent years.

This work does not analyze the impact of aerosols on changes in HEP due to the absence of a long-term record of aerosols concentration, we will further study this using model simulations.

Data Availability Statement

Data on hourly precipitation were obtained from the National Meteorological Information Center of the China Meteorological Administration, the best-track data of tropical cyclone were obtained from the China Meteorological Administration (http://tcdata.typhoon.org.cn/zjljsjj_zlhq.html), and the global reanalysis data set was provided by NCAR (https://psl.noaa.gov/data/gridded/data.ncep.reanalysis.html). The authors used MATLAB to perform calculations, SOMs analyses, and visualization.

References

Bao, M., & Wallace, J. M. (2015). Cluster analysis of Northern Hemisphere wintertime 500-hPa flow regimes during 1920–2014. *Journal of the Atmospheric Sciences*, *72*(9), 3597–3608. https://doi.org/10.1175/JAS-D-15-0001.1

Bolton, D. (1980). The computation of equivalent potential temperature. *Monthly Weather Review*, *108*(7), 1046–1053. https://doi.org/10.1175/1520-0493(1980)108<1046:TCOEPT>2.0.CO;2

Brooks, H. E., & Stensrud, D. J. (2000). Climatology of heavy rain events in the United States from hourly precipitation observations. *Monthly Weather Review*, *128*(4), 1194–1201. https://doi.org/10.1175/1520-0493(2000)128<1194:COHREI>2.0.CO;2

Chen, Y., Li, Y., & Zhao, T. (2015). Cause Analysis on Eastward Movement of Southwest China Vortex and Its Induced Heavy Rainfall in South China. *Advances in Meteorology*, *2015*, 1–22. http://doi.org/10.1155/2015/481735

Chiang, J., Swenson, L., & Kong, W. (2017). Role of seasonal transitions and the westerlies in the interannual variability of the East Asian summer monsoon precipitation. *Geophysical Research Letters*, *44*(8), 3788–3795. https://doi.org/10.1002/2017GL072739

Chou, C., & Chen, C.-A. (2010). Depth of convection and the weakening of tropical circulation in global warming. *Journal of Climate*, *23*(11), 3019–3030. https://doi.org/10.1175/2010JCLI3383.1

Davison, A. C., & Hinkley, D. V. (1997). *Bootstrap methods and their application* (p. 582). New York, NY: Cambridge University Press.

Ding, Y., & Chan, J. C. (2005). The East Asian summer monsoon: an overview. *Meteorology and Atmospheric Physics*, *89*(1–4), 117–142. https://doi.org/10.1007/s00703-005-0125-z

Emori, S., & Brown, S. (2005). Dynamic and thermodynamic changes in mean and extreme precipitation under changed climate. *Geophysical Research Letters*, *32*(17), L17706. https://doi.org/10.1029/2005GL023272

Gao, Q., Sun, Y., & You, Q. (2016). The northward shift of Meiyu rain belt and its possible association with rainfall intensity changes and the Pacific-Japan pattern. *Dynamics of Atmospheres and Oceans*, *76*(1), 52–62. https://doi.org/10.1016/j.dynatmoce.2016.08.005

Guo, J., Su, T., Li, Z., Miao, Y., Li, J., Liu, H., et al. (2017). Declining frequency of summertime local-scale precipitation over eastern China from 1970 to 2010 and its potential link to aerosols. *Geophysical Research Letters*, *44*(11), 5700–5708. https://doi.org/10.1002/2017GL073533

Hansen, J., Ruedy, R., Sato, M., & Lo, K. (2010). Global surface temperature change. *Reviews of Geophysics*, *48*(4) https://doi.org/10.1029/2010RG000345

Houze, R. A., Jr (2014). Cloud dynamics (Vol. 104, p. 496). Academic Press.

Johnson, N. C. (2013). How many ENSO flavors can we distinguish? *Journal of Climate*, *26*(13), 4816–4827. https://doi.org/10.1175/JCLI-D-12-00649.1

Jones, P., Lister, D., Osborn, T., Harpham, C., Salmon, M., & Morice, C. (2012). Hemispheric and large-scale land-surface air temperature variations: An extensive revision and an update to 2010. *Journal of Geophysical Research*, *117*(D5), D05127. https://doi.org/10.1029/2011JD017139

Kalnay, E., Kanamitsu, M., Kistler, R., Collins, W., Deaven, D., Gandin, L., et al. (1996). The NCEP/NCAR 40-year reanalysis project. *Bulletin of the American Meteorological Society*, *77*(3), 437–472. https://doi.org/10.1175/1520-0477(1996)077<0437:TNYRP>2.0.CO;2

Kendall, M. (1975). Rank correlation methods. 8, 4, (1–202). San Francisco, CA: The Jewish News of Northern California.

Kohonen, T. (2001). *Self-organizing maps* (p. 501). Springer. https://doi.org/10.1007/978-3-642-97610-0

Kohonen, T., Hynninen, J., Kangas, J., & Laaksonen, J. (1996). report*SOM_PAK: The self-organizing map program package (Report A31)* (p. 25). Helsinki University of Technology, Laboratory of Computer and Information Science. https://doi.org/10.1534/g3.114.012914

Kohonen, T., & Somervuo, P. (1998). Self-organizing maps of symbol strings. *Neurocomputing*, *21*(1–3), 19–30. https://doi.org/10.1016/S0925-2312(98)00031-9

Kong, W., Swenson, L. M., & Chiang, J. C. (2017). Seasonal transitions and the westerly jet in the Holocene East Asian summer monsoon. *Journal of Climate*, *30*(9), 3343–3365. https://doi.org/10.1175/JCLI-D-16-0087.1

Lawrimore, J. H., Menne, M. J., Gleason, B. E., Williams, C. N., Wuertz, D. B., Vose, R. S., & Rennie, J. (2011). An overview of the Global Historical Climatology Network monthly mean temperature data set, version 3. *Journal of Geophysical Research*, *116*(D19), D19121. https://doi.org/10.1029/2011JD016187

Lin, G.-F., & Chen, L.-H. (2006). Identification of homogeneous regions for regional frequency analysis using the self-organizing map. *Journal of Hydrology*, *324*(1–4), 1–9. https://doi.org/10.1016/j.jhydrol.2005.09.009

Li, M., Zhang, Q., & Zhang, F. (2016). Hail day frequency trends and associated atmospheric circulation patterns over China during 1960–2012. *Journal of Climate*, *29*(19), 7027–7044. https://doi.org/10.1175/JCLI-D-15-0500.1

Luo, Y., Wu, M., Ren, F., Li, J., & Wong, W.-K. (2016). Synoptic situations of extreme hourly precipitation over China. *Journal of Climate*, *29*(24), 8703–8719. https://doi.org/10.1175/JCLI-D-16-0057.1

Lupu, A., & Maenhaut, W. (2002). Application and comparison of two statistical trajectory techniques for identification of source regions of atmospheric aerosol species. *Atmospheric Environment*, *36*(36–37), 5607–5618. https://doi.org/10.1016/s1352-2310(02)00697-0

Mann, H. B. (1945). Nonparametric tests against trend. *Journal of the Econometric Society*, *13*(3), 245–259. https://doi.org/10.2307/1907187

Marchand, R., Beagley, N., Thompson, S. E., Ackerman, T. P., & Schultz, D. M. (2006). A bootstrap technique for testing the relationship between local-scale radar observations of cloud occurrence and large-scale atmospheric fields. *Journal of the Atmospheric Sciences*, *63*(11), 2813–2830. https://doi.org/10.1175/JAS3772.1

Miao, C., Sun, Q., Borthwick, A. G., & Duan, Q. (2016). Linkage between hourly precipitation events and atmospheric temperature changes over China during the warm season. *Scientific Reports*, *6*, 22543. (1), 1–13. https://doi.org/10.1038/srep22543

Parry, M., Parry, M. L., Canziani, O., Palutikof, J., Van der Linden, P., & Hanson, C. (2007). report*Climate change 2007-impacts, adaptation and vulnerability: Working group II contribution to the fourth assessment report of the IPCC*, (1–172). Cambridge University Press.

Rohde, R., Muller, R., Jacobsen, R., Muller, E., Perlmutter, S., Rosenfeld, A., et al. (2013). A new estimate of the average Earth surface land temperature spanning 1753 to 2011. *Geoinformatics & Geostatistics An Overview*, *1*(1), 2. https://doi.org/10.4172/2327-4581.1000101

Sen, P. K. (1968). Estimates of the regression coefficient based on Kendall's Tau. *Journal of the American Statistical Association*, *63*(324), 1379–1389. https://doi.org/10.1080/01621459.1968.10480934

Tao, S. Y. (1987). A review of recent research on the East Asian summer monsoon in China. (60–92). London: Oxford University Press.

Vallis, G. K., Zurita-Gotor, P., Cairns, C., & Kidston, J. (2015). Response of the large-scale structure of the atmosphere to global warming. *Quarterly Journal of the Royal Meteorological Society*, *141*(690), 1479–1501. https://doi.org/10.1002/qj.2456

Wang, B., & LinHo (2002). Rainy season of the Asian–Pacific summer monsoon. *Journal of Climate*, *15*(4), 386–398. https://doi.org/10.1175/1520-0442(2002)015<0386:RSOTAP>2.0.CO;2

Wang, X., & Liu, Y. (2017). Causes of extreme rainfall in May 2013 over Henan Province: the role of the southwest vortex and low-level jet. *Theoretical and Applied Climatology*, *129*, (1-2), 701–709. http://doi.org/10.1007/s00704-017-2054-4

Wang, Y., & Zhou, L. (2005). Observed trends in extreme precipitation events in China during 1961–2001 and the associated changes in large-scale circulation. *Geophysical Research Letters*, *32*(9), L09707. https://doi.org/10.1029/2005GL022574

You, Q., Liu, J., & Pepin, N. (2019). Changes of summer cloud water content in China from ERA-Interim reanalysis. *Global and Planetary Change*, *175*, 201–210. https://doi.org/10.1016/j.gloplacha.2019.02.014

Yu, R., & Li, J. (2012). Hourly rainfall changes in response to surface air temperature over eastern contiguous China. *Journal of Climate*, *25*(19), 6851–6861. https://doi.org/10.1175/JCLI-D-11-00656.1

Zhai, P., Zhang, X., Wan, H., & Pan, X. (2005). Trends in Total Precipitation and Frequency of Daily Precipitation Extremes over China. *Journal of Climate*, *18*, (7), 1096–1108. https://doi.org/10.1175/jcli-3318.1

Zhang, H., & Zhai, P. (2011). Temporal and spatial characteristics of extreme hourly precipitation over eastern China in the warm season. *Advances in Atmospheric Sciences*, *28*(5), 1177. https://doi.org/10.1007/s00376-011-0020-0

Zhang, Q., Ni, X., & Zhang, F. (2017). Decreasing trend in severe weather occurrence over China during the past 50 years. *Scientific Reports*, *7*(1), 42310. https://doi.org/10.1038/srep42310

Zhang, X., Jiang, H., Jin, J., Xu, X., & Zhang, Q. (2012). Analysis of acid rain patterns in northeastern China using a decision tree method. *Atmospheric Environment*, *46*, 590–596. https://doi.org/10.1016/j.atmosenv.2011.03.004